Evidence of interstitial-mediated boron self-diffusion in boron carbide

Guido Roma, Thomas Schuler

Graphical Abstract

Evidence of interstitial-mediated boron self-diffusion in boron carbide

Guido Roma, Thomas Schuler

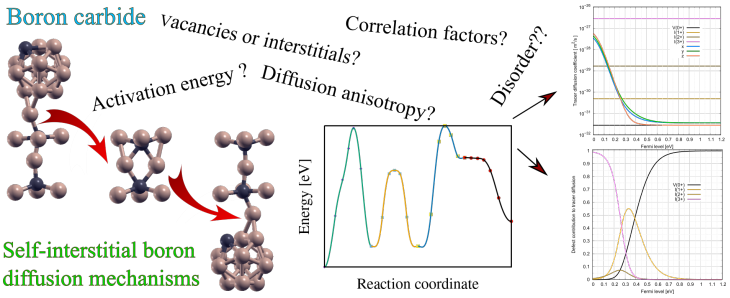

Highlights

Evidence of interstitial-mediated boron self-diffusion in boron carbide

Guido Roma, Thomas Schuler

- We highlight the importance of self-interstitial contribution to boron self-diffusion in boron carbide
- We provide prediction of diffusion coefficients as a function of temperature and Fermi level position

Evidence of interstitial-mediated boron self-diffusion in boron carbide

Guido Roma, Thomas Schuler

[a] *Université Paris-Saclay, CEA, Service de recherche en Corrosion et Comportement des Matériaux, SRMP, Gif sur Yvette, 91191, France*

Abstract

Boron carbide is an important high-temperature material with interesting structural and functional properties. However, self-diffusion is very poorly known on this material, and also the few impurity diffusion studies, devoted in particular to helium and lithium, overlook the possible diffusion coupling with intrinsic defects. In this paper we present a study of boron self-diffusion in boron carbide based on first principles calculations and kinetic cluster expansion. Our results show that boron self-diffusion may occur with a migration activation energy on the order of 1.5-1.6 eV and with a global activation energy between 4 and 5.5 eV, depending on the doping conditions, which is significantly lower than the self-diffusion activation energies in other semiconducting carbides, like silicon carbide.

We believe that our results are of interest for many applications of boron carbide and for tuning the best conditions for controlling the synthesis routes at specific stoichiometries for boron carbide.

Keywords: boron carbide, diffusion, first principles, DFT, point defects

1. Introduction

Boron carbide is a material which is both lightweight and very hard, which makes it suitable for applications in armors and ballistic protection in general [1] and for abrasives. It is a semiconductor envisaged as a thermoelectric material [2], as well as a cathode for Li-S batteries [3]. Moreover, due to the large neutron absorption cross section, and its smooth variation with energy, it is an absorber of choice in nuclear power plants of various types [4]. For improving its synthesis conditions, but also for many of the

mentioned applications, knowledge of self-diffusion properties in the material is very important.

For example, in nuclear applications, neutron irradiation produces, as in all materials, a supersaturation of point defects which can contribute to diffusion and other kinetic processes. In spite of various works devoted to characterisation of the irradiated material, including some discussing the role of electronic excitations [5], self-healing mechanisms before the amorphisation threshold [6, 7], and nanocluster formation [8], not much has been said concerning the diffusion of irradiation defects.

Concerning the synthesis of boron carbide, adding metal or metal oxide impurities helps the sintering process of boron carbide. Such beneficial effect was suggested to be related to enhanced diffusion, through a vacancy mechanism triggered by the formation of substoichiometric boron carbide [9, 10, 11]. However, this mechanisms was recently questioned due to the relative sintering aid efficiency of some metals and their oxides, highlighing instead the role of liquid phases induced by the presence of metals during sintering [12]. Moreover, two recent advances in the understanding of defect properties of boron carbide further exclude the role of vacancies: first, we now know that the contribution of vacancies to boron mobility cannot be significant, given the very large activation energy for vacancy diffusion (almost 4 eV) in this material [13]; second, substoichiometric (B-rich) boron carbide is not realized by introducing carbon vacancies, but boron icosahedral antisites and boron interstitials [14, 15].

Most studies related to diffusion in boron carbide have been conducted in the framework of nuclear applications, with a special interest in impurity diffusion: the kinetics of helium, which is produced in large quantities by neutron absorption reactions, was studied experimentally, mostly on materials irradiated in reactors, and with empirical models [16, 17, 18, 19, 20] already long ago. More recent works based on first principles calculations partly clarified the atomic mechanisms responsibles for helium diffusion and clustering[21, 13, 22].

Lithium impurities, which are also created by nuclear reactions, and their kinetics have been studied experimentally [23, 24] and, more recently, in a theoretical work which was limited to charge neutral interstitials [22].

For helium first principles calculations suggest a 2D diffusion regime, in $\langle 111 \rangle$ planes, activated at lower temperature than the 3D one,[21, 13] in agreement with the experimental observation of flat bubbles.[25, 26, 18, 27] A similar behaviour was found for lithium neutral [22] and charged [28] intersti-

tials. However, the picture of impurity diffusion is not complete without assessing possible coupling with the migration mechanisms of intrinsic defects. As far as vacancies are concerned, as we mentioned, at least for helium, we can exclude a diffusion enhancement through vacancy mechanisms. Interstitial mechanisms have not been scrutinized, except for neutral self-interstitials for which high migration barriers (> 3 eV) were reported [22]. However, boron interstitials, according to calculations, are most probably present in positively charged states (+1 to +3) [29]. Considering that lithium can be expected to be present in charge state +1 [28], a diffusion mechanism based on the exchange between boron and lithium interstitials, both of charge +1 to preserve the charge state, is fairly possible.

In this paper we investigate boron self-diffusion in B_4C boron carbide using first principles calculations. In Section 2 we describe the numerical tools used for this work, in Section 3.1 we describe the main jump mechanisms necessary to provide long-range diffusion of boron interstitials in perfectly ordered structures. In Section 3.2 we provide the values of boron self-diffusion coefficients resulting from these jump mechanisms, and in Section 3.3 we discuss the role of disorder in the distribution of polar icosahedral carbon atoms.

2. Approach, numerical tools, and material models

The results presented in this paper are based on density functional theory (DFT) calculations of migration barriers in B_4C boron carbide. The calculated energy barriers are further exploited through the kinetic cluster expansion approach implemented in the open-source KineCluE code [30, 31] in order to estimate self-diffusion coefficients, diffusion anisotropy and correlation coefficients.

2.1. First principles calculations

DFT calculations were carried out using the Quantum-Espresso software package [32, 33], based on plane waves and pseudopotentials. We used norm conserving pseudopotentials with an 80 Ry energy cutoff for describing electronic wavefunctions and the local density approximation (LDA) for the exchange correlation functional, which proved to give reliable results, very close to more sophisticated gradient corrected results, for this material [29].

Our material model is carbon-rich boron carbide with stoichiometry B_4C, whose unit cell contains 15 atoms arranged in a $B_{11}C$ icosahedron and a C-B-

C chain, the so-called $(B_{11}C^p)CBC$, where the p superscript indicates that the icosahedral carbon is in polar position. Although there are both experimental and theoretical hints that this structure might not be themodynamically reachable at finite temperature and ambient pressure [34, 35, 15], it is a good representation of most atomic scale features of boron carbide even at slightly less C-rich stoichiometries, and allows us to use a manageable supercell containing 120 atoms for the study of migration mechanisms. Within this supercell we described electronic screening by a rather well converged 3×3×3 Γ-centred **k**-point sampling grid. The equilibrium rhombohedric lattice parameter in our model is 5.059 Å with a slight monoclinic distortion (one angle of the monoclinic cell is 65.19 degrees and the other two are 66.13 degrees.

Structural relaxations were considered converged below a force threshold of 10^{-3} Ryd/Bohr. Calculations for supercells containing interstitial atoms were performed at constant volume. Migration barriers were obtained thanks to the Nudged-Elastic-Band (NEB) method [36], with a path error not exceeding 0.1 eV. For each NEB calculation we generally used 7 images with a climbing image. The interpolated NEB energy profiles shown in section 3 are obtained by the `path_interpolation.x` tool of Quantum-Espresso, which takes into account the forces tangent to the NEB path, which can give intermediate local minima. In our experience, when such minima are close in energy and position to the adjacent NEB images, they are fairly reliable.

Given the complexity of the energy landscape for some of the studied charge states, we also explored the energy landscape with the help of constrained relaxations using the generalized Bennett constraint [37]. For paths found in this way, we subsequently checked several portions of the path through NEB calculations between adjacent local minima. We did not use any automatic algorithm for path searching, but only educated guesses and trial and error.

We consider in this paper only positive charge states for boron interstitials, with charges +1, +2 and +3, which are the expected charge states within a wide range of Fermi level positions in boron carbide, and in particular in the p-type self-doping conditions, in which boron carbide is expected to be in thermodynamic equilibrium [29]. Charged defects are treated with the standard approach where a compensating uniform background is added in order to cope with a neutral system. When we mention formation energies, we add the monopole Madelung correction for the Coulomb interaction between periodic images. Otherwise, we focus on migration barriers, where all

configurations along a migration path would have, to first order in multipole expansion, the same correction.

2.2. From jump mechanisms to diffusion coefficients

Jump frequencies alone are not sufficient to compute diffusion coefficients because the exact manner in which these jump frequencies are linked to one another actually matters, as it gives rise to kinetic correlation effects. Therefore, for the calculation of diffusion coefficients, we use the open-source KineCluE code [30, 31] which automates the self-consistent mean field theory [38] to compute transport coefficients from the knowledge of the crystal structure, the available jump mechanisms and information about the energetic landscape of the system.

The KineCluE code operates on clusters which are defined as a small group of atoms or point defects located within some interaction radius from one another (here this interaction radius is set to 15 Å). The code fully takes into account the symmetry of the crystal. In this paper, we will consider the following clusters : isolated vacancy (V), vacancy-boron tracer pair ($V-\mathrm{B}^*$), interstitial boron atom (I, with various charge states) and interstitial-boron tracer pair ($I-\mathrm{B}^*$). The boron tracer atoms are identical to any other boron atom in the structure but marking them allows us to compute how fast a given atom diffuses in the structure, which defines the self-diffusion coefficients. We remind that the tracer diffusion coefficient is defined as the diffusion coefficient of a tagged atom at infinite dilution.

The code computes the kinetic correlations within each cluster and cluster transport coefficients are obtained from the configuration and migration energies associated with each jump mechanism. Then, from these transport coefficients and the cluster concentrations, we have access to the diffusion coefficients in any chosen direction. To calculate the cluster concentrations and then obtain self-diffusion coefficients from total transport coefficients, we will assume that point defects (V and I) are at equilibrium and use the formation energies provided in Table 1 for self-interstitial in various charge states and Ref. [13] for neutral vacancies. We have not computed the attempt frequencies for each migration step, so we chose to set the same value (20 THz) to each barrier, a value which is close to the frequency of chain pseudorotation modes [39, 40].

Dealing with a semiconductor, with a fairly large band gap, implies the presence of defects in various charge states. The kinetic cluster expansion approach has been slightly adapted to cope with charged defects [41]. In this

formalism the tracer diffusion coefficient reads :

$$D^*_{\mathrm{B}} = \frac{K_{V_0\mathrm{B}} D^*_{V_0\mathrm{B}} + K_{I_1\mathrm{B}} D^*_{I_1\mathrm{B}} + K_{I_2\mathrm{B}} D^*_{I_2\mathrm{B}} + K_{I_3\mathrm{B}} D^*_{I_3\mathrm{B}}}{1 + K_{V_0\mathrm{B}} + K_{I_1\mathrm{B}} + K_{I_2\mathrm{B}} + K_{I_3\mathrm{B}}}, \tag{1}$$

where $D^*_{d_q\mathrm{B}}$ represents the boron tracer diffusion coefficient mediated by defect d with charge q, as shown in Fig. 6 and $K_{d_q\mathrm{B}}$ is defined as:

$$K_{d_q\mathrm{B}} = Z_{d_q\mathrm{B}} \exp\left(-\frac{E_f(d_q) + q\mu_e}{k_B T}\right), \tag{2}$$

with μ_e being the electronic chemical potential with respect to the top of the valence band, $E_f(d_q)$ being the formation energy of a defect at the top of the valence band (as introduced earlier), and $Z_{d_q\mathrm{B}}$ is the interaction partition function between the defect and the tracer atom, which accounts for the configurational entropy and the energy of the various configurations. Note that there is no specific interaction between the defect and the tracer atom and therefore variations in energies only stem from the variety of sites accessible to the defect. This interaction partition function is also obtained from KineCluE.

3. Results

3.1. Boron interstitial configurations and elementary migration mechanisms

A summary of intrinsic point defects structural variants and formation energies in boron carbide is given in Ref. [29]. Concerning boron interstitials, which are the focus of this paper, we described them on the basis of the Wyckoff positions $2c$ and $6g$ of the rhombohedric $R\overline{3}m$ space group, which were used as a starting point for the structural relaxations of boron interstitials.

In principle, as the symmetry of the crystal is lower than that of the $R\overline{3}m$ space group —due to the presence of icosahedral carbon—, the 2 equivalent $2c$ positions of the $R\overline{3}m$ space group give rise to four inequivalent positions, two of which are twofold degenerate. In reality, in charge state +3 we found only three such configurations (see Fig.1). It is worthwhile to compare to the case of helium interstitials impurities, which is simpler: positions issued from the relaxation of helium inserted in $2c$ and $6g$ positions correspond to the interstitial positions dubbed type 2 and 3 in previous papers on helium diffusion [21, 13]. While for helium, hardly bonding to boron or carbon, the relaxed interstitial positions were very close (also in energy) to the ideal

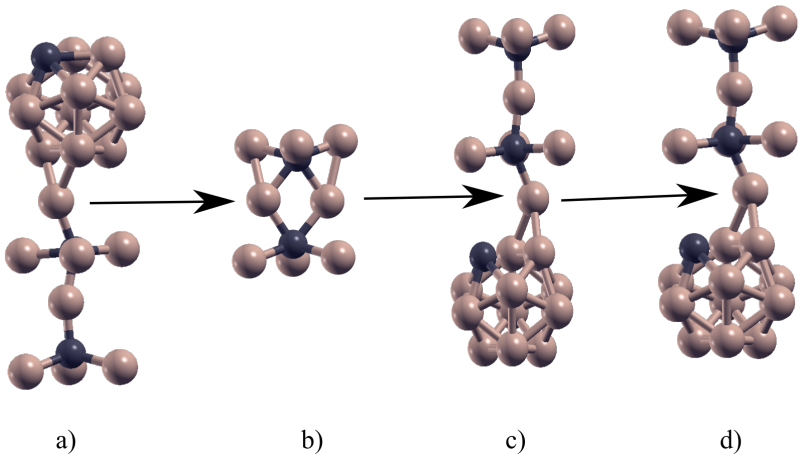

Figure 1: Configurations of a boron interstitial in charge state Q=+3. Boron atoms are brown, carbons are black. a) position $2c_B$ b) pantograph configuration c) position $2c_C^1$, d) position $2c_C^2$. The naming of configuration reflects the fact that, for $2C_B$ the closest icosahedral pole does not contain carbon, while for $2c_C^1$ and $2c_C^2$ the closest pole contains carbon. The arrows indicate the sequence of boron jumps for 2D diffusion, whose energy profile is given in figure 2.

Wyckoff positions, for boron the distortions are more pronounced, as can be seen from Fig. 1.

The interstitial relaxed from a $6g$ position reaches a pantograph like structure named C$\langle^{\rm B}_{\rm B}\rangle$C. Starting from a $2c$ position, while for helium leads to an interstitial impurity almost perfectly aligned with the nearby C-B-C chain [21], for boron leads to a more distorted structure, whose structural details also depend on the presence or not of carbon on the closest pole of the nearest icosahedron. This can be seen from the structures of the corresponding interstitials in the 3+ charge state shown in figure 1, which are the only four inequivalent structures that we could find for boron interstitials in charge state 3+. We note that charge state 3+ is the expected one in conditions of strong enough p-type doping.

While investigating the migration mechanisms between these configurations we realised that the $2c_C^1$ position is a very shallow local minimum, easily converted to the $2c_C^2$ configuration. We can then envisage a migration path starting from a conversion of the $2c_B$ to the pantograph like position; then, by an interstitialcy mechanisms, the other side of the pantograph can transform into a $2c_C^2$ configuration. The energy profile of such a mechanisms is

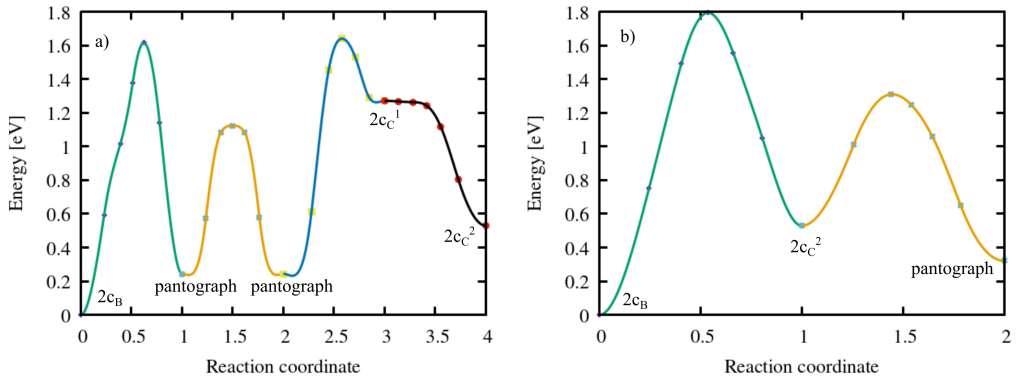

Figure 2: Energy profile for two sequences of jumps between various configurations of boron interstitials in charge state 3+. a) The profile, corresponding to a sequence leading to long range 2D diffusion, was obtained from four NEB calculations, providing transformations between the interstitial configurations shown in figure 1. The yellow curve is the (symmetric) energy profile for a rotation of the pantograph-like structure. b) This profile corresponds to two subsequent jumps allowing boron to diffuse in 3D, because here the three configurations are not in the same $\langle 111 \rangle$ slice. Points represent calculated NEB images, lines are interpolations.

given in figure 2a. This figure is obtained by four NEB calculations, the second one illustrates the rotation of the pantograph configuration ($\mathrm{C}\langle^{\mathrm{B_1}}_{\mathrm{B_2}}\rangle\mathrm{C} \rightarrow \mathrm{C}\langle^{\mathrm{B_2}}_{\mathrm{B_1}}\rangle\mathrm{C}$), a step which is skipped in the interstitialcy mechanism, but might be necessary for investigating isotopic effects on diffusion.

Such a migration sequence takes place in a $\langle 111 \rangle$ slice of the $(\mathrm{B_{11}C}^p)\mathrm{CBC}$ structure, meaning that it contributes to 2D diffusion, similarly to the helium 2D diffusion mechanism [21].

For 3D diffusion we investigated direct conversion between $2c_B$ and $2c_C$ configurations located in different $\langle 111 \rangle$ slices and found a jump mechanisms with barriers of 1.79 eV (forward) and 1.27 eV (backward) (figure 2b). Although the barrier for 3D diffusion is slightly higher than that for 2D diffusion, we are very far from the clearly distinct regimes found for helium and diffusion is expected to be close to isotropic. The reader might have remarked that the energy of the pantograph configuration in figure 2b is slightly higher (0.08 eV) than in figure 2a: we checked that the two configurations are virtually the same, as the barrier to go from the former to the latter is less than 0.01 eV and the potential energy surface between the two is very flat.

The situation gets even more complex when we switch to charge states

+2 and +1, which are expected for more moderate p-type conditions to intrinsic and even mild n-type doping [29]. For these two charge states we found additional equilibrium configurations, which show up as intermediate local minima along migration paths. These minima present structural motifs with a different or slightly different connectivity. For example, the boron interstitial can bind to form a $\mathrm{B}\langle^{\mathrm{C}}_{\mathrm{B}}\rangle\mathrm{B}$ structure involving one of the chain carbon atoms, together with the chain's boron and one of the icosahedral boron to which the C-B-C chain is bound. This can happen on both sides of the chain, with the poles of an icosahedron on the side containing a carbon atom (dubbed $\mathrm{B}\langle^{\mathrm{C}}_{\mathrm{B}}\rangle\mathrm{B}$ C-side or $\langle\mathrm{BCBB}\rangle_{\mathrm{C}}$) or not ($\mathrm{B}\langle^{\mathrm{C}}_{\mathrm{B}}\rangle\mathrm{B}$ B-side, or $\langle\mathrm{BCBB}\rangle_{\mathrm{B}}$). For the former we found two variants, slightly different in energy. Such bonding to the icosahedron leads to a sort of $\mathrm{B}_{12}\mathrm{C}$ cage structure, of which we show an example in figure 3, panels a) and b). These configurations are unstable in charge state Q+3 and, once relaxed, end up in one of the four structures presented inf figure 1. Other configurations include a T-like structure, where the interstitial boron is sitting on a line roughly perpendicular to the C-B-C chain and passing through the chain boron atom (figure 3c). Another variant features the boron interstitial sitting on the line passing through the centre of a CBBCBB hexagon and perpedicular to it, slightly displaced with respect to the hexagon's plane either towards a boron pole ($\mathrm{hex}_{\mathrm{B}}$) or a carbon one ($\mathrm{hex}_{\mathrm{B}}$), in figures 3d and 3e.

We summarize the configurations present in the various charge states, and their relative (formation) energies in Table 1, noting that, according to the charge state, some configurations can merge or are very similar. For example the T-like configuration is practically identical to the $2\mathrm{c}^2_{\mathrm{C}}$ configuration in charge state +2, while in charge state +1 the T-like configuration is close, but not identical, to a $2\mathrm{c}_{\mathrm{B}}$ configuration. Similarly, the $\mathrm{hex}_{\mathrm{C}}$ looks like a more or less distorted version of the $2\mathrm{c}^1_{\mathrm{C}}$ structure in charge state +2.

With several NEB calculations and constrained relations we devised, in the case of charge state Q=+2, a 3D diffusion mechanism for which the limiting step is the conversion from the $2\mathrm{c}_{\mathrm{B}}$ configuration to the $2\mathrm{c}^2_{\mathrm{C}}$ through the two hexagonal configurations, with a global energy barrier of 1.50 eV. For this charge state, such a path is favourable over our calculated 2D path, for which the barrier from $2\mathrm{c}_{\mathrm{B}}$ to the pantograph configuration (through a T-like intermediate structure) needs to overcome a barrier of 1.62 eV. We show the energy profile of both paths in figure 4.

Also for charge state Q=+1 the investigated paths show intermediate local minima. We could not find any favourable 2D migration pathway, in

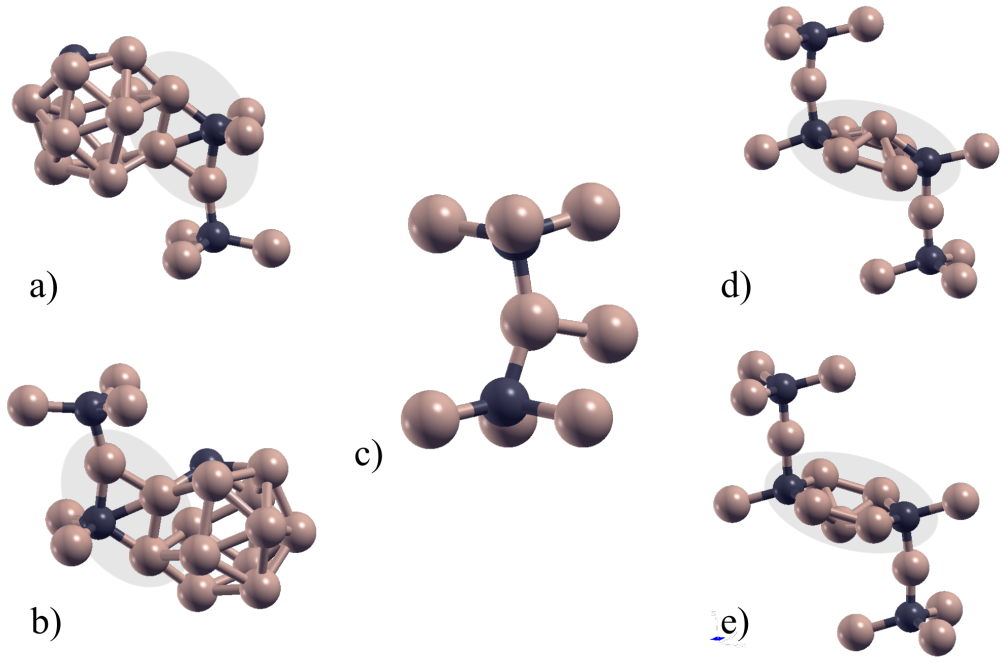

Figure 3: Additional stable configurations found in charge states Q=+2 and Q=+1 (boron atoms are brown, carbons black): a) B$\langle^{\mathrm{C}}_{\mathrm{B}}\rangle$B lozenge on the B-side of the icosahedron (the lozenze is highlighted), b) analogous configuration on the C-side of the icosahedron, c) T-like configuration at the C-B-C chain, d) hexagonal on the B-side of the icosahedron (or $\mathrm{hex_B}$, the hexagon is highlighted), e) analogous configuration on the C-side of the icosahedron. a) and b) are found only for charge state +1, while hexagonal configurations are found only for charge state +2. The T-like occurs in both charge states.

Type	Q=+1	Q=+2	Q=+3
$2c_B$	0.14 (3.43)	0.00 (3.00)	0.00 (2.52)
$C\langle^{B}_{B}\rangle C$	1.18 (4.47)	0.63 (3.63-3.64)	0.24 (2.76)
$2c^1_C$	1.55 (4.84)	1.22 (4.22-4.23)	1.27 (3.79)
$2c^2_C$	0.0 (3.29)	0.42 (3.42-43)	0.53 (3.05)
T-like	0.15 (3.44)	0.43 (3.43-3.52)	—
$B\langle^{C}_{B}\rangle B$ B-side	0.56 (3.85-3.91)	0.56 (3.56-3.63)	—
$B\langle^{C}_{B}\rangle B$ C-side	0.69 (3.75-3.98)	0.90 (3.90)	—
hex_B	—	0.98 (3.98)	—
hex_C	—	1.22 (4.22)	—

Table 1: List of the various configurations of boron interstitials found in the three studied charge states. We give energies relative to the lowest energy configuration of each charge state, and (in parenthesis) the formation energy in C-rich conditions and Fermi level at the valence band top (VBT). Some configuration are very close, though not identical, like, e.g., the $2c^1_C$ and the one dubbed hex_C or the T-like and the $2c^2_C$.

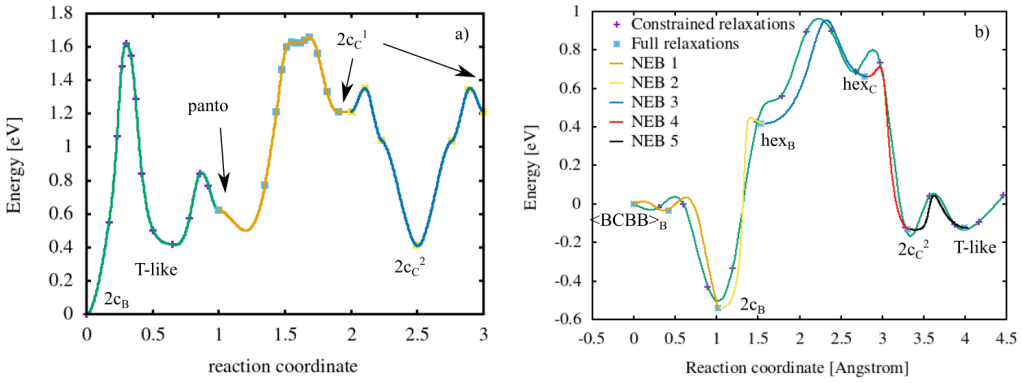

Figure 4: Energy profiles for a) 2D and b) 3D migration of a boron interstitial in charge state +2. We contructed the 3D path through successive constrained relaxations. The corresponding profile (green line) is shown together with NEB profiles of the various jumps, performed afterwards as a check between fully relaxed points (blue crosses). In this case the reaction coordinate, in Angstrom, is the one used for the constrained relaxation.

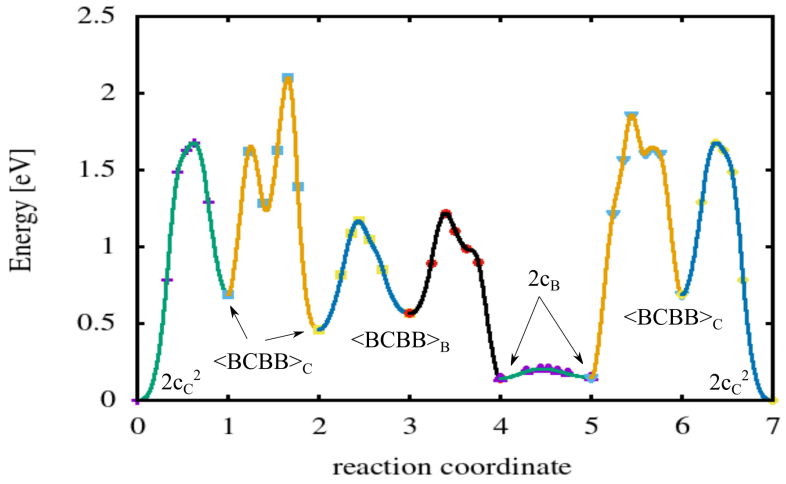

Figure 5: The long and tormented energy profile obtained for the migration of a boron interstitial in charge state +1. Each different color in the curve corresponds to a single NEB calculation. The second and the third of these steps correspond to interstitialcy mechanisms, where the moving boron atom replaces another boron of the pristine structure which, in turn, continues to migrate.

any case not more favourable than the pathway that we obtain by concatenating jumps along, approximately, one of the crystal axes connecting $2c_C^2$ positions through the following sequence: $2c_C^2 \rightarrow \langle BCBB\rangle_C \rightarrow \langle BCBB\rangle_C \rightarrow \langle BCBB\rangle_B \rightarrow 2c_B \rightarrow 2c_B \rightarrow \langle BCBB\rangle_C \rightarrow 2c_C^2$. The overall activation energy of this long path is 2.1 eV. The energy profile for this path is shown in figure 5. For this charge state we tested several possible paths, both through constrained relaxations and NEB calculations; many of the partial jumps possibly contributing to migration paths are interstitialcy mechanisms, where the migrating atom replaces a boron of the structure, which in turn starts migrating. Probably this is due to the fact that, in this charge state, the boron interstitial atoms seems to have a strong tendency to establish multiple bond with neighbouring atoms.

3.2. Boron self-diffusion in ordered B_4C

In order to predict boron self-diffusion in boron carbide we start by assuming an ordered crystalline structure with $(B_{11}C^p)CBC$ unit cell and we consider, for interstitials, the migration pathways described in the previous section and, for vacancies, the results given in Ref. [13]. The latter considers a direct jump between chain vacancy sites with a large energy barrier of 4.73

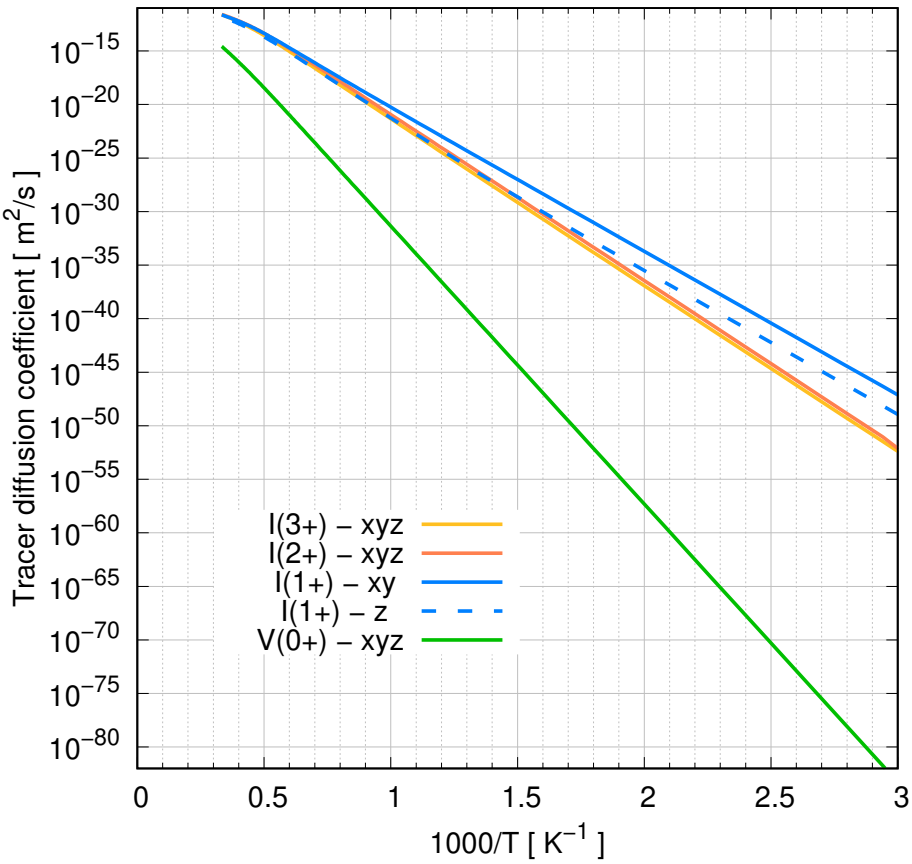

Figure 6: Tracer self-diffusion coefficients of boron atoms mediated by various defects.

eV, a mechanism passing through icosahedral polar site, with a lower though still high overall barrier of 3.72 eV, and a possible mechanism bypassing chain sites, with a lower barrier of 2 eV; the last mechanism is, however, penalised by the high formation energy, and weak dynamical stability, of polar vacancies.

This data is fed to the KineCluE code to obtain the tracer diffusion coefficients shown in Fig. 6. In all of the following, the "xyz" directions refer to a cartesian coordinate system in which the (111) plane of the B_4C unit cell is perpendicular to the z direction.

The diffusion coefficients displayed in Fig. 6 show Arrhenius behavior over the investigated temperature range. The parameters obtained by fitting these curves to an Arrhenius form are provided in Table 2. The $I(1+)$ defect

Defect type	Diffusion directions	Diffusion pre-factor	Activation energy	Migration energy
I(3+)	xyz	2.42×10^{-6}	4.20	1.68
I(2+)	xyz	3.14×10^{-6}	4.64	1.64
I(1+)	xy	3.90×10^{-7}	4.58	1.29
I(1+)	z	4.55×10^{-7}	4.76	1.47
V(0+)	xyz	2.35×10^{-6}	5.12	3.69

Table 2: Arrhenius parameters for boron tracer self-diffusion, obtained from fitting the values displayed in Fig. 6. When similar values were obtained for various directions, the value along the x direction is given. The last column is obtained by subtracting the formation energy of the defect from the activation energy. The energy values are given in eV and the diffusion pre-factors are in m^2/s.

is the only one which generates non-negligible diffusion anisotropy, with diffusion along the z direction being slightly slower than diffusion perpendicular to it. Diffusion mediated by the two other charge states of self-interstitial defect are less efficient at low temperature, but still much more efficient than vacancy-mediated diffusion. As we shall see later on, this conclusion is valid when the Fermi level is close enough to the top of the valence band (p-type conditions), but the vacancy contribution to tracer self-diffusion increases with the electron chemical potential, up to a point where it becomes dominant.

It is also of interest to look at kinetic correlation factors (Fig. 7). The correlation factor (between 0 and 1) is defined as the ratio between the actual diffusion coefficient and the ideal diffusion coefficient associated with a true random walk. The point defect itself can undergo correlated motion due to the various sites available to it and the non equivalent energy barriers between these sites (solid lines in Fig. 7). Moreover, there is another source of correlation arising when we follow the diffusion of a particular atom (the tracer atom) because most point-defect mediated diffusion mechanisms proceed in such a way that the displacement of the point defect is not always driven by the same atom, and therefore a given atom diffuses via successive association and dissociation jumps with the point defect. This behavior explains the difference between the tracer correlation factors (dashed lines in Fig. 7) and the point-defect correlation factors. Correlation factors for I(2+) are much lower than for other defects. This is because we included low-barrier jumps between local minima in some energy basin. These low

migration barriers increase the value of the ideal random walk diffusion coefficient, but because the jumps are all localized in an energy basin and do not participate in long-range diffusion, they introduce large kinetic correlation effects. In other words, the system oscillates very fast between these states, but these oscillations do not contribute to diffusion. The compensation between the low correlation factors and the fast ideal random diffusion can be seen in Fig. 6 : despite the large difference in correlation factors between defects I(2+) and I(3+), the tracer diffusion coefficients are very close to each other.

We now study the influence of the Fermi level position on the relative contributions of vacancies and self-interstitials to boron self-diffusion in B_4C. Figure 8 represents the evolution of the overall tracer diffusion coefficient as a function of the Fermi level, and the right hand side plot shows the relative contribution of each type of defect for diffusion in the x direction only, since the results are fairly isotropic. This curve was obtained using kinetic cluster expansion [42] including the specific formalism to deal with charged defects [41], as described in section 2.

First of all, Fig. 8 shows that diffusion is almost isotropic. Moreover, the tracer self-diffusion coefficient decreases from a value close to the $D^*_{I_{3+}\mathrm{B}}$ coefficient at $\mu_e = 0$ to the $D^*_{V_0\mathrm{B}}$ at higher μ_e values. This is further supported by the right hand side plot which shows that at low μ_e values, tracer diffusion is mainly mediated by self-interstitial defect with 3+ charge state, while at higher μ_e values, tracer diffusion is mediated by neutral vacancies.

Figure 9 shows that the same tendency is observed over the whole temperature range, but the magnitude of the decrease of the tracer self-diffusion coefficient between low and high μ_e values becomes less and less important as temperature increases, because $D^*_{d_q\mathrm{B}}$ coefficients get closer to each other, as seen in Fig. 6.

3.3. Influence of disorder on boron self-diffusion

Boron carbide is generally supposed to contain some sort of disorder. There are indications that one type of disorder is related to the distribution of carbon atoms on polar sites of the icosahedra. Previous works based on DFT suggest this [35, 43] and the low formation energy of antisite defects [29] is corroborating this view. The comparison of calculated Raman spectrum for a boron carbide model containing polar disorder with experimental spectra confirms this hypothesis [40]. In order to estimate the effect of disorder on boron self-diffusion we started from the 2D migration path of the interstitial

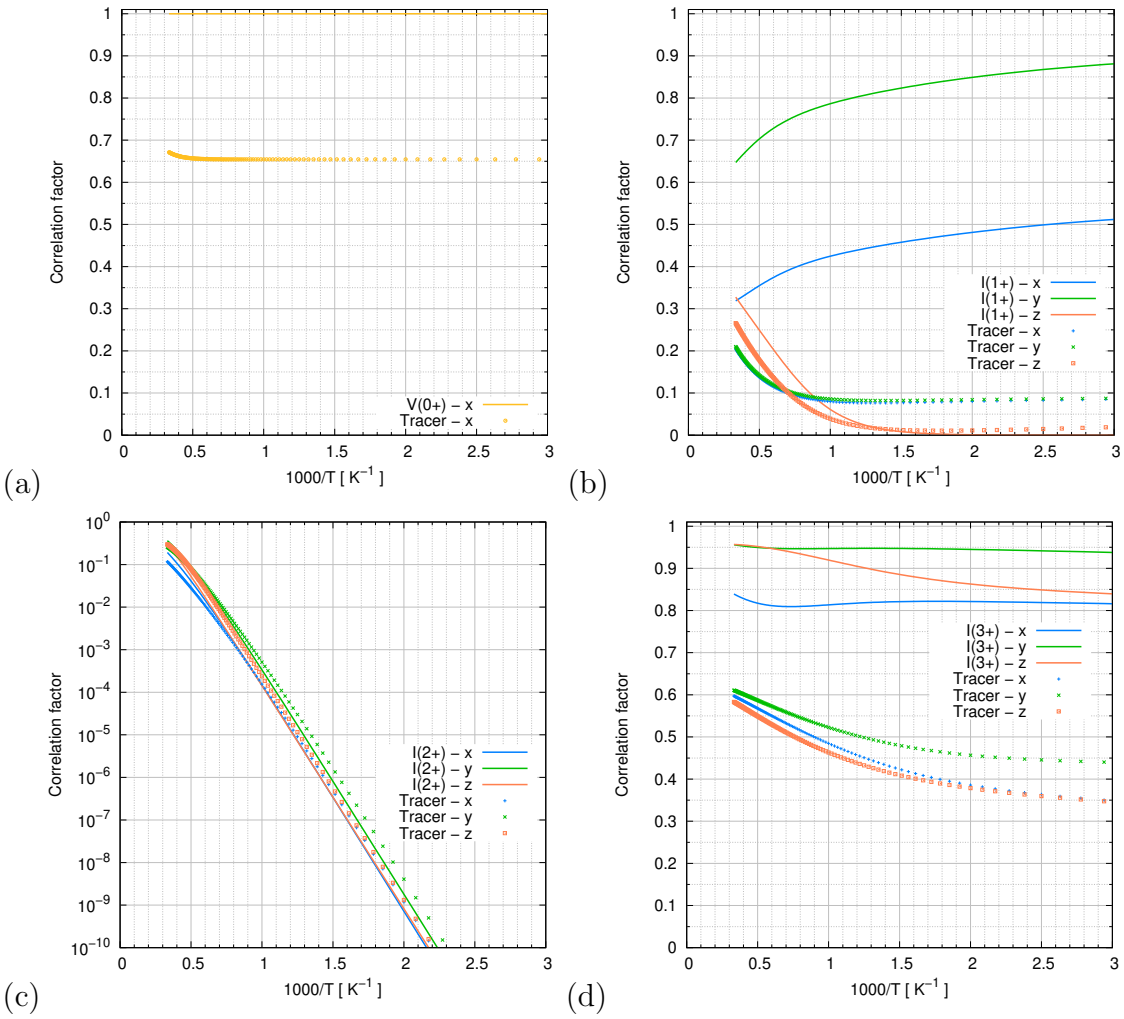

Figure 7: Correlation factors of an isolated defect and the tracer boron atom diffusing with that defect for various types of defects : neutral vacancy, which is isotropic (a); interstitial atom charged 3+ (b); interstitial atom charged 2+ (c); interstitial atom charged 1+ (d). Vacancy diffusion is not correlated, whatever the diffusion direction.

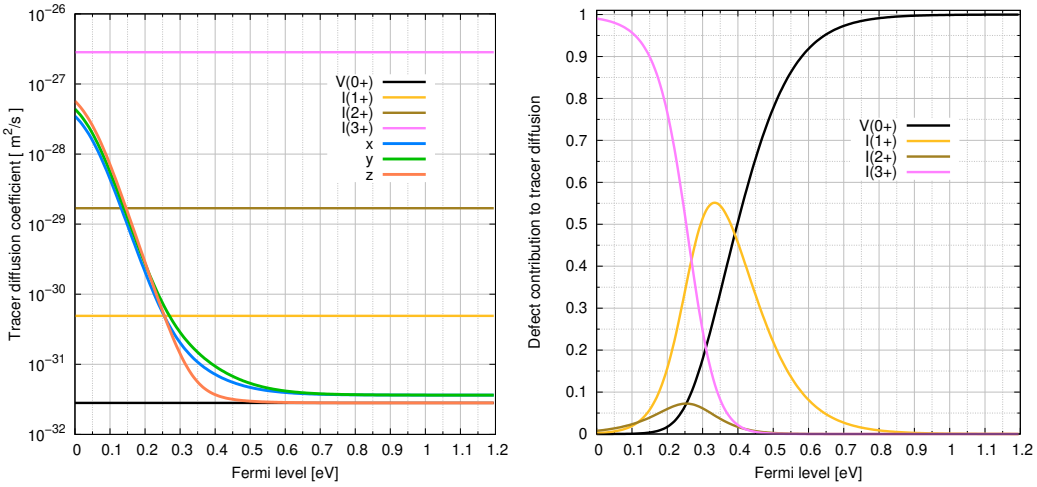

Figure 8: The left hand side plot shows the overall tracer self-diffusion coefficient computed from Eq. 1 as a function of the Fermi level μ_e at T=1000 K. The horizontal lines show the diffusion coefficients obtained independently for each defect at the same temperature in the z direction. The right hand side plot shows the relative importance of each defect contribution to the diffusion of boron atoms.

in charge state +3 (figure 2) and, for each of the three minima (1=2c_B, 2=pantograph, and 3=2c_C^1), we chose three close icosahedral poles containing carbon and constructed configurations by permuting the polar atoms. We relaxed those configurations and performed NEB calculations as for the first and third steps in figure 2. We note that the relaxations, especially in charge states +2 and +1, might end up in configurations relatively far from the starting positions and, as a consequence, the NEB paths might contain intermediate minima (or shrink into a single point), and the paths might not be sufficient to provide long range diffusion. However, we think they might provide a first assessment of the role of disorder on boron self-diffusion.

We analysed the outcoming migration energy profiles and extracted the global barrier (difference between the highest energy in the path and the lowest minimum in the sequence of the two jumps). We plot them as a function of the distance traveled by the migrating boron atom in figure 10 (without considering the width of the pantograph intermediate configuration).

In the case of charge state +1 many of those calculations (including the one for the ordered structure) end up in uncoverged results or large energy barriers, probably due to the fact that the considered path, initially found for the Q=+3 charge state, does not take into account the necessary boron atom

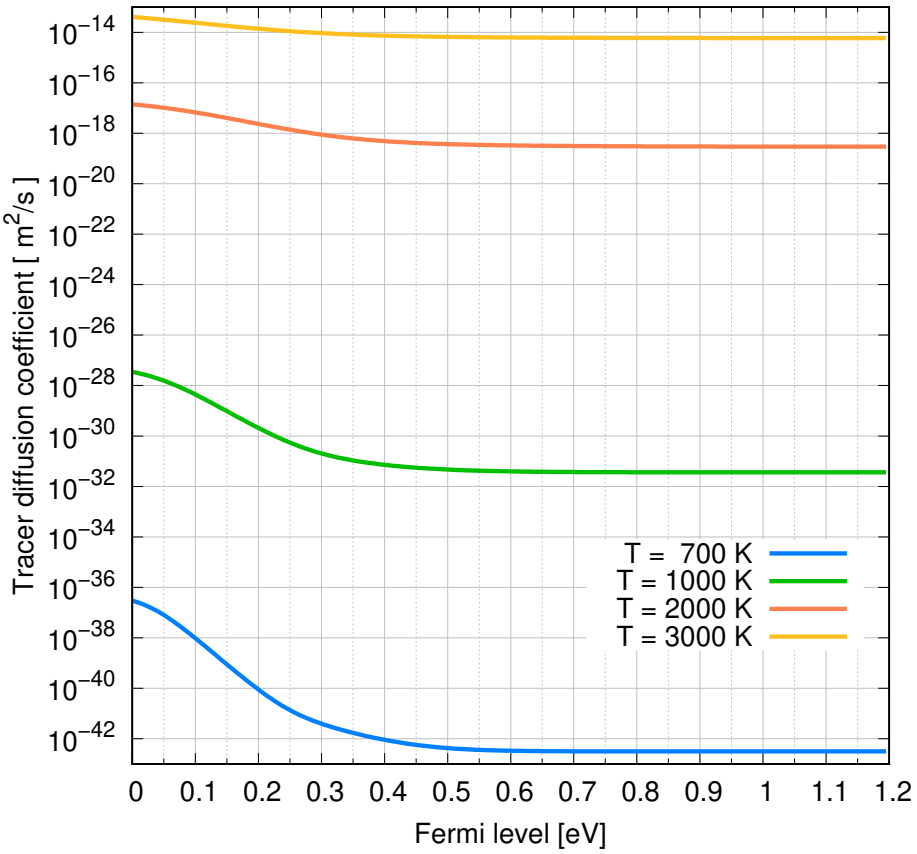

Figure 9: Boron tracer self-diffusion coefficient obtained for various temperatures as a function of the Fermi level. Diffusion coefficients are represented only along the x direction because, as shown in Fig. 8, diffusion is nearly isotropic.

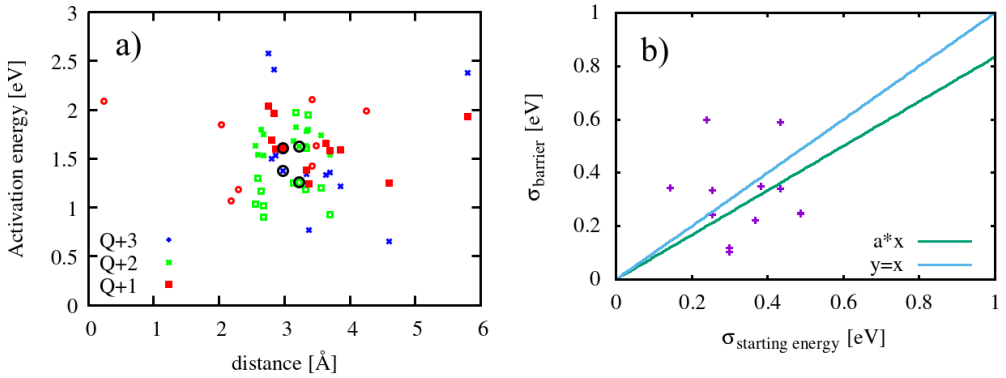

Figure 10: a) Global energy barriers for the two step interstitialcy diffusion shown in figure 2 when some polar carbon disorder is added to the B_4C structure. b) standard deviation of groups of energy barriers as a function of the standard deviation of the energy of the respective starting configuration. The two full lines are a fit of the data to a function $f(x) = ax$ (green line) and the reference curve $y(x) = x$ (blue line). Values for the ordered structure are circled in black.

exchanges typical of interstitialcy mechanisms. We remind that vacancies have much higher migration energies, out of the range of figure 10. We thus take into account only interstitials in charge states Q=+2 and Q=+3 in the following very simple analysis: we consider the standard deviation of the calculated energy barriers and of the corresponding starting points, both for the partial jumps and for the global barriers obtained from the combination of the two jumps (shown in figure 10a). The results are shown in panel b) of figure 10. The rationale in doing this comparison is related to the findings about diffusion in disordered media according to which the uncorrelated similarity between site disorder and barrier disorder leads to an Arrhenius type behaviour [44], with an activation energy which, at high temperature, tends to the average barrier, but at low temperature is closer to the lowest available barrier. In our case the two standard deviations are of similar order of magnitude, but not always very close. Still, a partial compensation between site and barrier disorder, in the spirit of Ref. [44] is expected.

Of course a more detailed analysis of possible correlations between site and barrier energies would be necessary in order to predict activation energies in presence of disorder, however our analysis supports the idea that the activation energies calculated in the ordered $(B_{11}C)CBC$ crystal are a fairly

reliable estimation for boron self-diffusion in boron carbide.

4. Conclusion

We have presented in this paper a theoretical study of boron self-diffusion in boron carbide based on first principles DFT calculations coupled with the kinetic cluster expansion approach.

The B_4C structure is quite complicated, with multiple local energy minima for self-interstitial atoms, depending on the charge state. We have computed a fair number of these local minima and energy barriers between them (in fact many more than those presented in figures 2,4 and 5), but we cannot rule out the possibility that we have missed some configurations and/or jump mechanisms leading to a more efficient diffusion of tracer atoms. Moreover, we have assumed that the structure was perfectly ordered regarding the distribution of C atoms on polar sites of the icosaedron, and that the system was stoichiometric. Strictly speaking, our conclusions are only valid under these assumptions, although we do not expect the activation energies will change too much.

Our results show that the contribution of interstitial boron to self-diffusion is dominant with respect to vacancy contribution when the material is in strong enough *p*-type conditions. Without any doubt, given the migration part of the activation energies, the interstitial mechanism is the one to consider in conditions of supersaturation of interstitials, e.g. under irradiation or even, most probably, in boron rich conditions. Our results should, inter alia, guide the search for optimal boron carbide synthesis conditions. We hope that our study will spark further interest in diffusion in boron carbide, in particular in carbon self-diffusion and the diffusion of various impurities, which in many cases we expect to be coupled with self-interstitial kinetics.

5. Acknowledgements

The CNRS NEEDS programme is gratefully aknowledged for funding of the project CIAN, in the framework of which this work was partially carried on.

This work was granted access to the HPC resources of TGCC and IDRIS under the allocations 2022-A0130906018 and 2021-A0110906018 made by GENCI.

References

[1] M. Boldin, N. Berendeev, N. Melekhin, A. Popov, A. Nokhrin, V. Chuvildeev, Review of ballistic performance of alumina: Comparison of alumina with silicon carbide and boron carbide, Ceramics International 47 (18) (2021) 25201–25213. doi:https://doi.org/10.1016/j.ceramint.2021.06.066.
URL https://www.sciencedirect.com/science/article/pii/S0272884221018058

[2] T. L. Aselage, High Temperature Thermoelectric Properties of Boron Carbide, MRS Online Proceedings Library (OPL) 234 (1991) 145. doi:10.1557/PROC-234-145.

[3] L. Luo, S.-H. Chung, H. Yaghoobnejad Asl, A. Manthiram, Long-Life Lithium–Sulfur Batteries with a Bifunctional Cathode Substrate Configured with Boron Carbide Nanowires, Advanced Materials 30 (39) (2018) 1804149. arXiv:https://onlinelibrary.wiley.com/doi/pdf/10.1002/adma.201804149, doi:https://doi.org/10.1002/adma.201804149.
URL https://onlinelibrary.wiley.com/doi/abs/10.1002/adma.201804149

[4] D. Gosset, 15 - Absorber materials for Generation IV reactors, in: P. Yvon (Ed.), Structural Materials for Generation IV Nuclear Reactors, Woodhead Publishing, 2017, pp. 533–567. doi:https://doi.org/10.1016/B978-0-08-100906-2.00015-X.
URL https://www.sciencedirect.com/science/article/pii/B978008100906200015X

[5] G. Victor, Y. Pipon, N. Bérerd, N. Toulhoat, N. Moncoffre, N. Djourelov, S. Miro, J. Baillet, N. Pradeilles, O. Rapaud, A. Maître, D. Gosset, Structural modifications induced by ion irradiation and temperature in boron carbide B_4C, Nuclear Instruments and Methods in Physics Research Section B: Beam Interactions with Materials and Atoms 365 (2015) 30–34, proceedings of the 19th International Conference on Ion Beam Modification of Materials (IBMM 2014). doi:https://doi.org/10.1016/j.nimb.2015.07.082.
URL https://www.sciencedirect.com/science/article/pii/S0168583X15006606

[6] D. Gosset, S. Miro, S. Doriot, N. Moncoffre, Amorphisation of boron carbide under slow heavy ion irradiation, Journal of Nuclear Materials

476 (2016) 198–204. doi:https://doi.org/10.1016/j.jnucmat.2016.04.030.
URL https://www.sciencedirect.com/science/article/pii/S0022311516301441

[7] Y. Pipon, G. Victor, N. Moncoffre, G. Gutierrez, S. Miro, T. Douillard, O. Rapaud, N. Pradeilles, P. Sainsot, N. Toulhoat, M. Toulemonde, Structural modifications of boron carbide irradiated by swift heavy ions, Journal of Nuclear Materials 546 (2021) 152737. doi:https://doi.org/10.1016/j.jnucmat.2020.152737.
URL https://www.sciencedirect.com/science/article/pii/S0022311520313453

[8] M. N. Mirzayev, A. A. Donkov, E. A. Popov, E. Demir, S. H. Jabarov, L. S. Chkhartishvili, S. A. Adeojo, A. S. Doroshkevich, A. A. Sidorin, A. G. Asadov, T. T. Thabethe, M. U. Khandaker, S. Alamri, H. Osman, A. V. Trukhanov, S. V. Trukhanov, Modeling and X-ray Analysis of Defect Nanoclusters Formation in B_4C under Ion Irradiation, Nanomaterials 12 (15) (2022). doi:10.3390/nano12152644.
URL https://www.mdpi.com/2079-4991/12/15/2644

[9] L. Levin, N. Frage, M. P. Dariel, The effect of Ti and TiO_2 additions on the pressureless sintering of B_4C, Metallurgical and Materials Transactions A 30 (12) (1999) 3201–3210. doi:10.1007/s11661-999-0230-6.
URL https://doi.org/10.1007/s11661-999-0230-6

[10] K. Sairam, J. Sonber, T. Murthy, C. Subramanian, R. Hubli, A. Suri, Development of B_4C–HfB_2 composites by reaction hot pressing, International Journal of Refractory Metals and Hard Materials 35 (2012) 32–40. doi:https://doi.org/10.1016/j.ijrmhm.2012.03.004.
URL https://www.sciencedirect.com/science/article/pii/S0263436812000546

[11] T. S. R. C. Murthy, J. K. Sonber, K. Sairam, R. Bedse, J. Chakarvartty, Development of Refractory and Rare Earth Metal Borides & Carbides for High Temperature Applications, Materials Today: Proceedings 3 (9, Part B) (2016) 3104–3113, advances in Refractory and Reactive Metals and Alloys (ARRMA 2016). doi:https://doi.org/10.1016/j.matpr.2016.09.026.
URL https://www.sciencedirect.com/science/article/pii/S2214785316303017

[12] E. A. Weaver, B. T. Stegman, R. W. Trice, J. P. Youngblood, Mechanical properties of room-temperature injection molded, pressurelessly

sintered boron carbide, Ceramics International 48 (8) (2022) 11588–11596. doi:https://doi.org/10.1016/j.ceramint.2022.01.015.
URL https://www.sciencedirect.com/science/article/pii/S0272884222000165

[13] K. Gillet, G. Roma, J.-P. Crocombette, D. Gosset, The influence of irradiation induced vacancies on the mobility of helium in boron carbide, J. Nucl. Mater. 512 (2018) 288–296. doi:https://doi.org/10.1016/j.jnucmat.2018.10.020.

[14] K. Rasim, R. Ramlau, A. Leithe-Jasper, T. Mori, U. Burkhardt, H. Borrmann, W. Schnelle, C. Carbogno, M. Scheffler, Y. Grin, Local Atomic Arrangements and Band Structure of Boron Carbide, Angewandte Chemie International Edition 57 (21) (2018) 6130–6135, _eprint: https://onlinelibrary.wiley.com/doi/pdf/10.1002/anie.201800804.
doi:https://doi.org/10.1002/anie.201800804.
URL https://onlinelibrary.wiley.com/doi/abs/10.1002/anie.201800804

[15] A. Jay, O. Hardouin Duparc, J. Sjakste, N. Vast, Theoretical phase diagram of boron carbide from ambient to high pressure and temperature, Journal of Applied Physics 125 (18) (2019) 185902, _eprint: https://doi.org/10.1063/1.5091000. doi:10.1063/1.5091000.
URL https://doi.org/10.1063/1.5091000

[16] J. C. Clayton, W. A. Bostrom, F. C. Schrag, The release of helium from slightly irradiated boron carbide and boron carbide-silicon carbide plates, Tech. Rep. WAPD-255, Washington, D.C. (1962).
URL http://hdl.handle.net/2027/mdp.39015095062918

[17] C. E. Beyer, G. W. Hollenberg., S. A. Duran, A physically based model for helium release from irradiated boron carbide, Tech. Rep. HEDL-SA-1833-FP (1979).

[18] T. Stoto, J. Ardonceau, L. Zuppiroli, M. Castiglioni, B. Weckermann, Behaviour of implanted helium in boron carbide in the temperature range 750 to 1720
textdegree C, Radiation Effects 105 (1-2) (1987) 17–30. doi:10.1080/00337578708210059.

[19] V. V. Svetukhin, D. N. Suslov, V. D. Risovanyi, P. F. Salikh-zade, Mechanisms of helium thermodesorption from irradiated boron carbide, Atomic Energy 98 (2005) 177.

[20] V. Motte, D. Gosset, T. Sauvage, H. Lecoq, N. Moncoffre, Helium apparent diffusion coefficient and trapping mechanisms in implanted B_4C boron carbide, J. Nucl. Mater. (2019). doi:https://doi.org/10.1016/j.jnucmat.2019.02.012.
URL http://www.sciencedirect.com/science/article/pii/S0022311518308201

[21] A. Schneider, G. Roma, J.-P. Crocombette, V. Motte, D. Gosset, Stability and kinetics of helium interstitials in boron carbide from first principles, J. Nucl. Mater. 496 (2017) 157 – 162.

[22] Y. You, K. Yoshida, T. Yano, First-principles investigation of neutron-irradiation-induced point defects in B_4C, a neutron absorber for sodium-cooled fast nuclear reactors, Japanese Journal of Applied Physics 57 (5) (2018) 055801. doi:10.7567/JJAP.57.055801.
URL https://dx.doi.org/10.7567/JJAP.57.055801

[23] X. Deschanels, D. Simeone, J. P. Bonal, Determination of the lithium diffusion coefficient in irradiated boron carbide pellets, Journal of Nuclear Materials 265 (3) (1999) 321–324. doi:https://doi.org/10.1016/S0022-3115(98)00887-3.
URL https://www.sciencedirect.com/science/article/pii/S0022311598008873

[24] Y. You, K. Yoshida, T. Inoue, T. Yano, Helium bubbles and trace of lithium in B_4C control rod pellets used in JOYO experimental fast reactor, Journal of Nuclear Science and Technology 55 (6) (2018) 640–648. arXiv:https://doi.org/10.1080/00223131.2017.1419889, doi:10.1080/00223131.2017.1419889.
URL https://doi.org/10.1080/00223131.2017.1419889

[25] A. Jostsons, C. DuBose, G. Copeland, J. Stiegler, Defect structure of neutron irradiated boron carbide, Journal of Nuclear Materials 49 (2) (1973) 136–150. doi:10.1016/0022-3115(73)90003-2.

[26] G. W. Hollenberg, B. Mastel, J. A. Basmajian, Effect of Irradiation Temperature on the Growth of Helium Bubbles in Boron Carbide, Journal of the American Ceramic Society 63 (1980) 376–380. doi:10.1111/j.1151-2916.1980.tb10195.x.

[27] V. Motte, D. Gosset, G. Gutierrez, S. Doriot, N. Moncoffre, Helium cluster nucleation and growth in implanted

B_4C boron carbide, J. Nucl. Mater. 514 (2019) 334–347. doi:https://doi.org/10.1016/j.jnucmat.2018.12.012.

[28] G. Roma, Mobilité du lithium dans le carbure de bore, Rapport Annuel SRMP, p. 47 (2021).

[29] G. Roma, K. Gillet, A. Jay, N. Vast, G. Gutierrez, Understanding first-order Raman spectra of boron carbides across the homogeneity range, Phys. Rev. Materials 5 (2021) 063601. doi:10.1103/PhysRevMaterials.5.063601.
URL https://link.aps.org/doi/10.1103/PhysRevMaterials.5.063601

[30] T. Schuler, L. Messina, M. Nastar, Kineclue: A kinetic cluster expansion code to compute transport coefficients beyond the dilute limit, Computational Materials Science 172 (2020) 109191. doi:https://doi.org/10.1016/j.commatsci.2019.109191.
URL https://www.sciencedirect.com/science/article/pii/S0927025619304902

[31] T. Schuler, L. Messina, M. Nastar, Kineclue v1.0 github repository (2019).
URL https://github.com/lukamessina/kineclue

[32] P. Giannozzi, S. Baroni, N. Bonini, M. Calandra, R. Car, C. Cavazzoni, D. Ceresoli, G. L. Chiarotti, M. Cococcioni, I. Dabo, A. D. Corso, S. d. Gironcoli, S. Fabris, G. Fratesi, R. Gebauer, U. Gerstmann, C. Gougoussis, A. Kokalj, M. Lazzeri, L. Martin-Samos, N. Marzari, F. Mauri, R. Mazzarello, S. Paolini, A. Pasquarello, L. Paulatto, C. Sbraccia, S. Scandolo, G. Sclauzero, A. P. Seitsonen, A. Smogunov, P. Umari, R. M. Wentzcovitch, QUANTUM ESPRESSO: a modular and open-source software project for quantum simulations of materials, J. Phys.: Condens. Matter 21 (2009) 395502.
URL http://stacks.iop.org/0953-8984/21/i=39/a=395502

[33] P. Giannozzi, O. Andreussi, T. Brumme, O. Bunau, M. B. Nardelli, M. Calandra, R. Car, C. Cavazzoni, D. Ceresoli, M. Cococcioni, N. Colonna, I. Carnimeo, A. D. Corso, S. de Gironcoli, P. Delugas, R. A. D. J. A. Ferretti, A. Floris, G. Fratesi, G. Fugallo, R. Gebauer, U. Gerstmann, F. Giustino, T. Gorni, J. Jia, M. Kawamura, H.-Y. Ko, A. Kokalj, E. Küçükbenli, M. Lazzeri, M. Marsili, N. Marzari, F. Mauri, N. L. Nguyen, H.-V. Nguyen, A. O. de-la Roza, L. Paulatto,

S. Poncé, D. Rocca, R. Sabatini, B. Santra, M. Schlipf, A. P. Seitsonen, A. Smogunov, I. Timrov, T. Thonhauser, P. Umari, N. Vast, X. Wu, S. Baroni, Advanced capabilities for materials modelling with Quantum ESPRESSO, J. Phys.: Condens. Matter 29 (2017) 465901. doi:10.1088/1361-648X/aa8f79.
URL http://www.quantum-espresso.org

[34] H. Okamoto, B-C (boron-carbon), Journal of Phase Equilibria 13 (4) (1992) 436–436. doi:10.1007/BF02674994.
URL https://doi.org/10.1007/BF02674994

[35] W. P. Huhn, M. Widom, A Free Energy Model of Boron Carbide, Journal of Statistical Physics 150 (3) (2013) 432–441. doi:10.1007/s10955-012-0642-3.
URL https://doi.org/10.1007/s10955-012-0642-3

[36] G. Henkelman, B. P. Uberuaga, H. Jónsson, A climbing image nudged elastic band method for finding saddle points and minimum energy paths, The Journal of Chemical Physics 113 (22) (2000) 9901–9904. doi:10.1063/1.1329672.
URL https://doi.org/10.1063/1.1329672

[37] G. Roma, J.-P. Crocombette, Evidence for a kinetic bias towards antisite formation in SiC nano-decomposition, J. Nucl. Mater. 403 (2010) 32–41. doi:http://dx.doi.org/10.1016/j.jnucmat.2010.06.001.

[38] M. Nastar, V. Y. Dobretsov, G. Martin, Self-consistent formulation of configurational kinetics close to equilibrium: The phenomenological coefficients for diffusion in crystalline solids, Philosophical Magazine A 80 (1) (2000) 155–184. arXiv:https://doi.org/10.1080/01418610008212047, doi:10.1080/01418610008212047.
URL https://doi.org/10.1080/01418610008212047

[39] A. Jay, Conception in silico d'une nouvelle phase de carbure de bore, Ph.D. thesis, Ecole Doctorale Polytechnique (2015).

[40] G. Roma, A. Jay, N. Vast, O. H. Duparc, G. Gutierrez, Reply to "comment on 'understanding first-order raman spectra of boron carbides across the homogeneity range' ", Phys. Rev. Materials 6 (2022) 016602.

doi:10.1103/PhysRevMaterials.6.016602.
URL https://link.aps.org/doi/10.1103/PhysRevMaterials.6.016602

[41] E. Haurat, J.-P. Crocombette, T. Schuler, M. Tupin, Hydrogen diffusion coefficient in monoclinic zirconia in presence of oxygen vacancies, International Journal of Hydrogen Energy 47 (78) (2022) 33517–33529. doi:10.1016/j.ijhydene.2022.07.216.
URL https://doi.org/10.1016/j.ijhydene.2022.07.216

[42] T. Schuler, M. Nastar, L. Messina, Mass-transport properties of ternary Fe(C,O) alloys revealed by multicomponent cluster synergies, Physical Review Materials 4 (2) (Feb. 2020). doi:10.1103/physrevmaterials.4.020401.
URL https://doi.org/10.1103/physrevmaterials.4.020401

[43] A. Ektarawong, S. I. Simak, L. Hultman, J. Birch, B. Alling, First-principles study of configurational disorder in B_4C using a superatom-special quasirandom structure method, Phys. Rev. B 90 (2014) 024204. doi:10.1103/PhysRevB.90.024204.
URL https://link.aps.org/doi/10.1103/PhysRevB.90.024204

[44] Y. Limoge, J.-L. Bocquet, Temperature Behavior of Tracer Diffusion in Amorphous Materials: A Random-Walk Approach, Phys. Rev. Lett. 65 (1990) 60.